We P 22

Computation of Optimized Arrays for 3-D Electrical Imaging Surveys

M.H. Loke (Geotomo Software), P.B. Wilkinson* (British Geological Survey) & J.C. Chambers (British Geological Survey)

SUMMARY

Three-dimensional surveys and inversion models are required to accurately resolve structures in areas with very complex geology where 2-D models might suffer from artifacts. Many 3-D surveys use a survey grid where the number of electrodes along one direction (x) is much greater than in the perpendicular direction (y). Frequently, due to limitations in the number of independent electrodes in the multi-electrode system, the surveys use a roll-along system with a small number of parallel survey lines aligned along the x-direction. The 'Compare R' array optimization method previously used for 2-D surveys is adapted for such 3-D surveys. Offset versions of the inline arrays used in 2-D surveys are included in the number of possible arrays (the comprehensive data set) to improve the sensitivity to structures in between the lines. By using PCs with modern graphics cards incorporating a fast Graphics Processing Unit (GPU) and using an improved single-precision 'Compare R' algorithm, the 3-D optimized arrays can be calculated within a reasonable time despite the comprehensive data set possibly have millions of arrays. A comparison with data sets using inline measurements made using conventional arrays show that structures located between the lines are much better resolved with the optimized arrays.

Introduction

Within the last 20 years, 2-D resistivity surveys have emerged as one of the main tools to map areas with moderately complex geology (Auken et al., 2006). However, in areas with very complex geology, the models obtained from 2-D surveys can suffer from artifacts due to off-line structures. For such problems, 3-D surveys using a rectangular grid of electrodes provide the best solution (Gharibi and Bentley, 2005; Chambers et al., 2006). In recent years, there has been significant progress in algorithms to automatically determine optimized arrays that will maximize the subsurface resolution of data from 2-D surveys (Wilkinson et al., 2012). The 'Compare R' method that directly calculates the model resolution proved to be the best method (Wilkinson et al., 2006). A fast version of this method using the microcomputer Graphics Processing Unit (GPU) was implemented by Loke et al. (2010). However, 3-D surveys present new challenges due to the large number of possible arrays that can run into millions. To meet this challenge, a combination of improvements in the software algorithm, GPU hardware and innovative measurement techniques is used.

Method

(a) An improvement to the 'Compare R' method

The smoothness-constrained least-squares optimization method is frequently used for 2-D and 3-D inversion of resistivity data (Loke et al., 2003). The linearized least-squares equation that gives the relationship between the model parameters (**r**) and the data misfit (**g**) is given below.

$$\left(\mathbf{G}^{\mathrm{T}}\mathbf{G}+\lambda\mathbf{C}\right)\Delta\mathbf{r}_{\mathbf{i}}=\mathbf{G}^{\mathrm{T}}\mathbf{g}-\lambda\mathbf{C}\,\mathbf{r}_{\mathbf{i-1}}, \quad (1)$$

The Jacobian matrix **G** contains the sensitivities of the (logarithms of the) apparent resistivities with respect to the model resistivity values, **C** contains the roughness filter constraint and λ is a damping factor. The model resolution matrix **R** (Loke et al., 2010) is given by

$$\mathbf{R}=\mathbf{B}\ \mathbf{A}\ \text{, where}\ \mathbf{A}=\mathbf{G}^{\mathrm{T}}\mathbf{G}\ \text{ and }\ \mathbf{B}=\left(\mathbf{A}+\lambda\mathbf{C}\right)^{-1} \quad (2)$$

The main diagonal elements of **R** give the model cells resolutions. The 'Compare R' method attempts to determine the set of arrays that maximizes the average resolution value for a homogeneous earth model. For a system with *N* electrodes, there are $N(N\text{-}1)(N\text{-}2)(N\text{-}3)/8$ independent four-electrode configurations. To reduce the number of possible arrays, arrays with the Wenner-γ type configuration and those large geometric factors are excluded (Stummer et al., 2004). A local optimization procedure is used to select a subset of the viable configurations (the comprehensive data set) that will maximize the model resolution. A small base data set consisting of the dipole-dipole configurations with an '*a*' spacing of 1 unit and '*n*' values of 1 to 8 is initially selected. The change in the model resolution matrix **R** for each new array added to the base set is calculated. A specified number of configurations that give the largest increases in the model resolution is then added to the base set. This is repeated until the desired number of optimized array configurations is selected. The following formula is used to calculate the change in the resolution matrix **ΔR** when a new array is added to the base set.

$$\Delta\mathbf{R}=\frac{\mathbf{z}}{1+\mu}\left(\mathbf{g}^{\mathrm{T}}-\mathbf{y}^{\mathrm{T}}\right), \text{ where } \mathbf{y}=\mathbf{Az},\ \mathbf{z}=\mathbf{Bg} \text{ and } \mu=\mathbf{g}.\mathbf{z}. \quad (3)$$

Loke et al. (2010) showed that carrying out the calculations using single-precision mathematics is about twice as fast as using double-precision. However, there was a small difference in the results (of less than 5%) obtained using single and double precision mathematics. In this paper, a small modification is made to the method used to calculate elements of the **A** matrix to greatly reduce the difference. The **A** matrix elements are calculated using the following relationship.

$$a(i,j)=\sum_{k=1}^{k=n}g(k,i).g(k,j) \quad (4)$$

Each element is the sum of *n* values from the product of the Jacobian matrix elements. As *n* can be large, particularly for the comprehensive data set, it is calculated using double precision to reduce round-off errors. The elements are of the **A** matrix (stored in double precision) are used to calculate the model resolution in equation (2). However it leads to a small inconsistency if the calculation of **ΔR** is carried out in single precision. To remove this inconsistency, the elements of the **A** matrix are

rounded down to single precision before calculating **ΔR**. With this modification, the optimized arrays calculated using single precision are almost identical to those obtained using double precision.

(b) Improvements in GPU hardware

A very efficient method to calculate **ΔR** simultaneously for a large number of test arrays using the GPU is described in (Loke et al., 2010). It was found that a major computational speed limitation was the rate at which data can be transferred between the main computer memory (RAM) and the graphics card memory (VRAM). One recent development is the PCI-E 3.0 graphics card bus system that is twice as fast as the older PCI-E 2.0 system. To illustrate the speed improvement, calculations were carried out on two PCs for optimized arrays for 2-D surveys lines ranging from 80 to 120 electrodes. The first PC has a Nvidia 560GTX PCI-E 2.0 graphics card, while the second has a Nvidia 670GTX PCI-E 3.0 graphics card. The newer graphics card system reduces the calculation time by about 40% (Table 1).

(c) Creating the comprehensive data set for 3-D surveys

The time taken by the 'Compare R' method is proportional to the number of arrays in the comprehensive data set (n_c). As n_c is proportional to the fourth power of the number of electrode positions, it would appear that the 'Compare R' method is impractical for 3-D survey grids. However, many 3-D surveys use an arrangement where the number of electrodes along one ('*x*') direction is much larger than in the perpendicular ('*y*') direction. One example is shown in Figure 1 with 3 cables with 21 electrodes each (Dahlin et al., 2002). A larger area can be surveyed by moving the setup in the *y* direction using a roll-along method, such as the 21 by 17 survey grid used by Dahlin et al. (2002). Although the final survey grid has 357 electrodes, not all possible combinations of the electrodes can be used. The method used to generate the comprehensive data set for 2-D survey lines is modified for such an arrangement with several parallel lines. The comprehensive data set consists of arrays with the alpha and beta configurations, such as those shown in Figures 2a and 2f. For a given number of electrode positions along a survey line, all viable inline alpha and beta configurations can be easily generated. In addition to the inline array, an offset version of the array where the potential electrodes are shifted to the next line is also generated (Figure 2b). A similar double offset version of the array is also generated (Figure 2c). Figure 2d shows another possible variation where the electrodes are distributed on three different lines. Similarly for each inline beta array, offset versions (Figures 2g,h,i) versions are also generated. The same selected maximum geometric factor is used to select the viable offset arrays. The rationale for using the offset versions of the inline arrays is illustrated in Figure 3 in the form of the sensitivity patterns at a horizontal plane at a depth of 0.1 m. The highest positive and negative sensitivity values for the inline alpha array (Figure 3a) are concentrated near the array axis, and does not extend more than 1 meter in the *y* direction from the array axis. The sensitivity pattern for the alpha array with the single offset potential electrodes (Figure 3b) shows much larger sensitivity values in the region between the two lines. Extending the offset to 2 meters increases the areas with the large sensitivity values between the y=0 and y=2 lines (Figure 3c). The triple line alpha array configuration (Figure 3d) has a similar sensitivity pattern to the inline array except the pattern is orientated in a diagonal direction between the lines. The different offset versions of the beta array configuration (Figure 3g,h,i) show a similar pattern with larger sensitivity values between the lines. For survey systems where the electrodes in 4 different lines can be used at the same time, a 'quadruple line' array type is included in the comprehensive data set (Figures 2e and 2j). These configurations (Figures 3e,j) have high sensitivity values in a diagonal pattern between the 4 lines.

Results

We present the results for a synthetic test model. The model consists of three rectangular blocks with resistivity of 1000 ohm.m at different depths embedded in a homogeneous medium of 100 ohm.m (Figure 4). The survey grid consists of 8 lines with 21 electrodes each. The inline electrode spacing is 1 meter while the distance between the lines is 2 meters. We first calculate the apparent resistivity values for the inline Wenner-Schlumberger and dipole-dipole arrays where the geometric factor is less than 2262 m. The second data set was created by the 'Compare R' array optimization method. Voltage dependent Gaussian random noise (Zhou and Dahlin, 2003) with an amplitude of 1 milli-ohm was added to the resistance values before they were converted into apparent resistivity values. The L1-norm method was used for both the data misfit and model roughness (Loke et al., 2003) in the

inversion of this data. The L-curve method was used to estimate the optimum inversion damping factor. Figure 4 shows the inversion models for the conventional arrays (with 3152 data points) and the optimized data (3154 data points) sets. The optimized data set has slightly more points to maintain symmetry in the array configurations used. The top two blocks are poorly resolved by the conventional arrays data set (Figure 4a) compared to the optimized data set (Figure 4b). The width of the topmost block anomaly (Figure 4a) is twice the actual size while its maximum resistivity is less than 240 ohm.m. In comparison, the optimized arrays inversion model has a maximum resistivity of about 640 ohm.m (Figure 4b) and the correct width. The poor performance of the conventional arrays data set is due to the poor sensitivity in the region between the lines (Figures 3a,f) of the inline arrays. The offset arrays included in the optimized data set have much higher sensitivities in this region. The optimized arrays also achieve significantly higher resistivity values at the locations of the second and the third blocks. Note that although the data misfit for the optimized data set (0.66%) is slightly higher than that for the conventional data set (0.34%) due to the higher average geometric factor of the optimized arrays, the model resolution is better.

Conclusions

We show that by combining improvements to the software algorithm, new GPU hardware and an innovative method to generate the arrays in the comprehensive data set, the 'Compare R" method can be used to generate optimized arrays for 3-D surveys that perform better than conventional arrays.

References

Auken, E., Pellerin, L., Christensen, N.B. and Sørensen, K. [2006] A survey of current trends in near-surface electrical and electromagnetic methods. *Geophysics*, **71**, G249-G260.

Chambers, J.C., Kuras, O., Meldrum, P.I., Ogilvy, R.D. and Hollands, J. [2006] Electrical resistivity tomography applied to geologic, hydrogeologic, and engineering investigations at a former waste-disposal site. *Geophysics*, **71**, B231-B239.

Dahlin, T., Bernstone, C. and Loke, M.H. [2002] A 3D resistivity investigation of a contaminated site at Lernacken in Sweden. *Geophysics*, **60**, 1682-1690.

Gharibi, M. and Bentley, L.R. [2005] Resolution of 3-D electrical resistivity images from inversions of 2-D orthogonal lines. *Journal of Environmental and Engineering Geophysics*, **10**, 339-349.

Loke, M.H., Acworth, I. and Dahlin, T. [2003] A comparison of smooth and blocky inversion methods in 2D electrical imaging surveys. *Exploration Geophysics*, **34**, 182-187.

Loke, M.H., Wilkinson, P.W. and Chambers, J.E. [2010] Parallel computation of optimized arrays for 2-D electrical imaging. *Geophysical Journal International*, **183**, 1202-1315.

Stummer, P., Maurer, H. and Green, A. [2004] Experimental design: Electrical resistivity data sets that provide optimum subsurface information. *Geophysics*, **69**, 120-129.

Wilkinson, P.B., Meldrum, P.I., Chambers, J.E., Kuras, O. and Ogilvy, R.D. [2006] Improved strategies for the automatic selection of optimized sets of electrical resistivity tomography measurement configurations. *Geophysical Journal International*, **167**, 1119-1126.

Wilkinson, P.B., Loke, M.H., Meldrum, P.I., Chambers, J.E., Kuras, O., Gunn, D.A. and Ogilvy, R.D. [2012] Practical aspects of applied optimised survey design for Electrical Resistivity Tomography. *Geophysical Journal International*, **189**, 428-440.

Zhou, B. and Dahlin, T. [2003] Properties and effects of measurement errors on 2D resistivity imaging surveying. *Near Surface Geophysics*, **1**, 105-117.

Table 1 *Time required to generate 15000 data points for 2-D survey lines using different GPUs.*

Number of electrodes	Comprehensive data set size	Number of model cells	560GTX Time (s.)	670GTX Time (s.)
80	2867265	2210	12227	7091
100	6965447	2940	43164	24581
120	14329228	3875	138341	79820

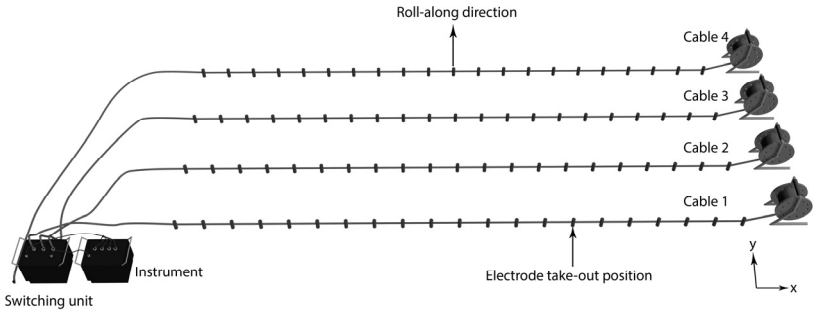

Figure 1 *Arrangement of survey lines using a 3 cable system with the Abem SAS instrument.*

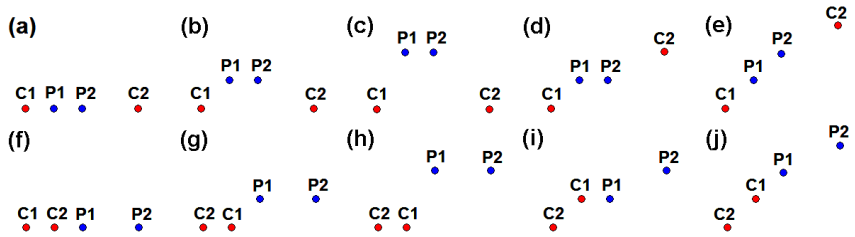

Figure 2 *Arrangement of alpha type array with (a) inline, (b) single offset, (c) double offset, (d) triple line and (e) quadruple line configurations. Beta type array arrangement with (f) inline, (g) single offset, (h) double offset and (i) triple line and (j) quadruple line configurations.*

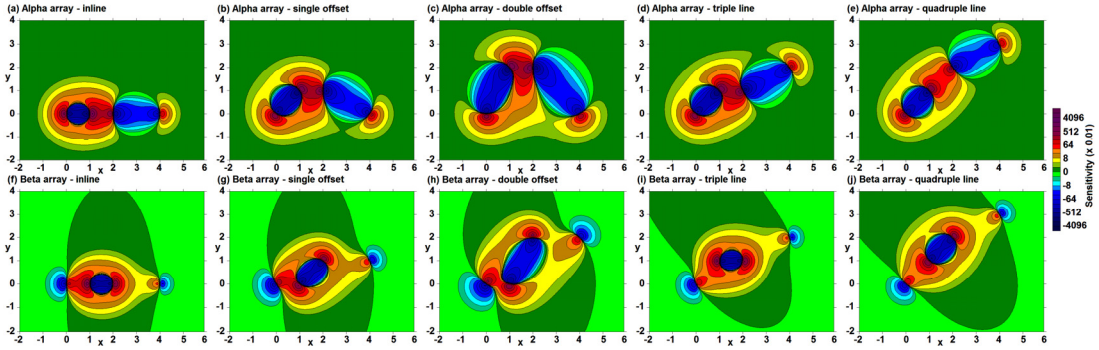

Figure 3 *Sensitivity patterns at a depth of 0.1 meter for alpha type array with (a) inline, (b) single offset, (c) double offset, (d) triple line and (e) quadruple line configurations. Similar sensitivity patterns for beta type array with (f) inline, (g) single offset, (h) double offset, (i) triple line and (j) quadruple line configurations. The unit electrode spacing is 1 m.*

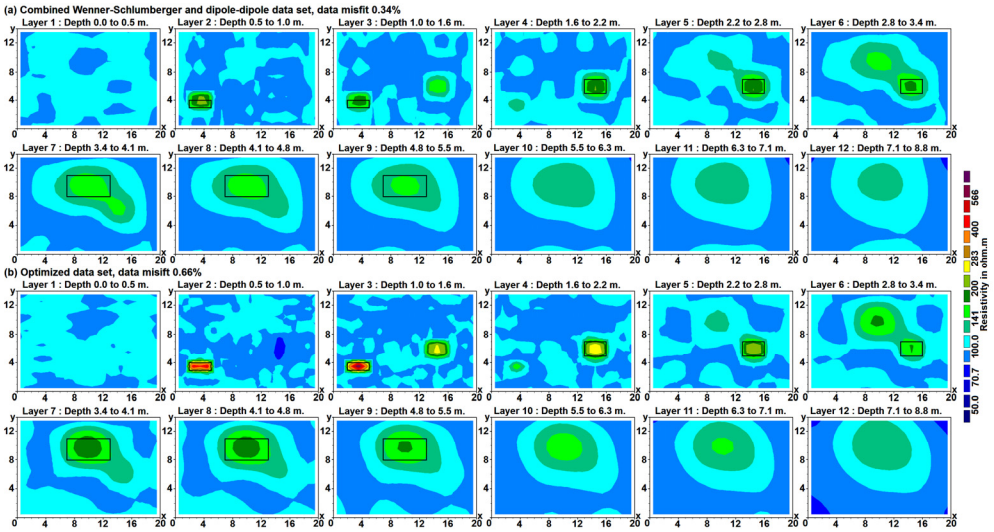

Figure 4 *Inversions model for (a) combined Wenner-Schlumberger and dipole-dipole data set, (b) optimized data set. The actual positions of the blocks are marked by black rectangles.*